



## Crystal structure of a novel putative sugar isomerase from the psychrophilic bacterium *Paenibacillus* sp. R4

Sunghark Kwon<sup>a</sup>, Hyun Ji Ha<sup>b</sup>, Yong Jun Kang<sup>b</sup>, Ji Hye Sung<sup>b</sup>, Jisub Hwang<sup>c, d</sup>,  
Min Ju Lee<sup>c</sup>, Jun Hyuck Lee<sup>c, d, \*\*</sup>, Hyun Ho Park<sup>b, \*</sup>

<sup>a</sup> Department of Biotechnology, Konkuk University, Chungju, Chungbuk, 27478, Republic of Korea

<sup>b</sup> College of Pharmacy, Chung-Ang University, Dongjak-gu, Seoul, 06974, Republic of Korea

<sup>c</sup> Research Unit of Cryogenic Novel Material, Korea Polar Research Institute, Incheon, 21990, Republic of Korea

<sup>d</sup> Department of Polar Sciences, University of Science and Technology, Incheon, 21990, Republic of Korea



### ARTICLE INFO

#### Article history:

Received 21 October 2021

Accepted 7 November 2021

Available online 11 November 2021

#### Keywords:

Sugar isomerase

Xylose isomerase

Glucose isomerase

*Paenibacillus*

Psychrophilic bacteria

Cold adaptation

### ABSTRACT

Sugar isomerases (SIs) catalyze the reversible conversion of aldoses to ketoses. A novel putative SI gene has been identified from the genome sequence information on the psychrophilic bacterium *Paenibacillus* sp. R4. Here, we report the crystal structure of the putative SI from *Paenibacillus* sp. R4 (*PbSI*) at 2.98 Å resolution. It was found that the overall structure of *PbSI* adopts the triose-phosphate isomerase (TIM) barrel fold. *PbSI* was also identified to have two heterogeneous metal ions as its cofactors at the active site in the TIM barrel, one of which was confirmed as a Zn ion through X-ray anomalous scattering and inductively coupled plasma mass spectrometry analysis. Structural comparison with homologous SI proteins from mesophiles, hyperthermophiles, and a psychrophile revealed that key residues in the active site are well conserved and that dimeric *PbSI* is devoid of the extended C-terminal region, which tetrameric SIs commonly have. Our results provide novel structural information on the cold-adaptable SI, including information on the metal composition in the active site.

© 2021 Elsevier Inc. All rights reserved.

### 1. Introduction

Sugar isomerases (SIs) reversibly catalyze the conversion of aldoses to ketoses. Xylose isomerases (XIs; a type of SI), also known as glucose isomerases catalyze the isomerization of D-xylose and D-glucose to D-xylulose and D-fructose, respectively [1]. XIs have become popular in the food industry because they can be efficiently used for high-fructose corn syrup production without forming any by-products [2,3]. Moreover, xylulose is used as a fermentation source for ethanol production in the biofuel industry, and the conversion of xylose to xylulose by this process can be achieved using XIs [4,5]. XIs also have catalytic activity for other sugars such as D-ribose, D-allose, and L-arabinose besides D-xylose and D-glucose [6].

SIs including XIs adopt the triose-phosphate isomerase (TIM) barrel fold structure, primarily exhibiting the tetrameric form as a

functional unit [7–12]. They also have metal cofactors for catalysis in the active site [1,13]. The metal cofactors comprise two divalent cations such as Mg<sup>2+</sup>, Mn<sup>2+</sup>, and Co<sup>2+</sup> [1,13], one of which contributes to substrate fixation and the other is directly involved in hydride shift [14]. Despite these generalized roles of the metal ions, SIs show a diversity of metal species depending on host organisms [1]. Moreover, the heterogeneity or homogeneity of metal composition needs to be confirmed to understand the specific roles of the respective metal ions. Therefore, metal preference identification for the cofactor is necessary for characterization of a novel SI.

To date, numerous studies on SIs, including XIs, have revealed their structures and mechanisms of action [15–18]. However, these primarily included the SIs from mesophilic and thermophilic bacteria. Studies conducted on SIs from psychrophilic bacteria are rare [19]. Such limited research has resulted in a scarcity of structural and functional information on SIs from psychrophilic bacteria.

**Abbreviations:** SI, sugar isomerase; *PbSI*, sugar isomerase from *Paenibacillus* sp. R4; TIM, triose-phosphate isomerase; XI, xylose isomerase; *PbXI*, xylose isomerase from *Paenibacillus* sp. R4; *StXI*, xylose isomerase from *Salmonella typhimurium*; *TtXI*, xylose isomerase from *Thermus thermophilus*; *TtsXI*, xylose isomerase from *Thermoanaerobacterium thermosulfurigenes*; SEC-MALS, size exclusion chromatography-coupled multi-angle light scattering; ICP-MS, inductively coupled plasma mass spectrometry.

\*\* Corresponding author. Research Unit of Cryogenic Novel Material, Korea Polar Research Institute, Incheon, 21990, Republic of Korea.

\* Corresponding author. College of Pharmacy, Chung-Ang University, Dongjak-gu, Seoul, 06974, Republic of Korea.

E-mail addresses: [junhyucklee@kopri.re.kr](mailto:junhyucklee@kopri.re.kr) (J.H. Lee), [xrayleox@cau.ac.kr](mailto:xrayleox@cau.ac.kr) (H.H. Park).

Structural and functional studies on novel SIs from psychrophilic bacteria can provide valuable information on determinants for contribution to protein cold adaptation. A putative SI gene has previously been identified based on the genome sequence of the psychrophilic bacterium *Paenibacillus* sp. R4, which was isolated from ice in Antarctica [19]. The putative SI from *Paenibacillus* sp. R4 (PbSI) was selected for elucidation of its crystal structure and structural features.

Herein, we present the crystal structure of PbSI at 2.98 Å resolution. Structural analysis revealed the TIM barrel fold as a main architecture. Our anomalous X-ray scattering along with inductively coupled plasma mass spectrometry (ICP-MS) indicates that PbSI has a Zn ion and a Ca ion in the active site. In addition, structural comparative analysis implies that a unique topology of PbSI and biophysical properties thereof may be associated with cold adaptation. Our results contribute to expansion of structural information on TIM barrel proteins, including the metal species in the active site.

## 2. Materials and methods

### 2.1. Vector construction, overexpression, and purification

Using the polymerase chain reaction, the gene encoding PbSI was amplified from the genomic DNA of *Paenibacillus* sp. R4 with a forward primer (5'-CTGCCATATGGAACGTTTACAAACATAGA-3') and a reverse primer (5'-CTGGCTCGAGTTACACATGCTCCAAATATC-3') (the underlined sequences indicate the *Nde*I and *Xho*I restriction sites, respectively). The amplified gene products were ligated into pET-28a vectors (Novagen, Madison, WI, USA) having the same restriction sites. The recombinant expression vectors with a hexa-His tag and a thrombin protease recognition site at the N terminus were delivered into *Escherichia coli* BL21(DE3) cells for protein mass production. The transformed cells were cultured in lysogeny broth medium containing 50 µg/mL kanamycin. When the optical density at 600 nm reached 0.5, 0.5 mM isopropyl-1-thio-β-D-galactopyranoside was added to the medium for induction, and the cells were further cultured overnight at 25 °C. Thereafter, cells were collected by centrifugation at 6000 rpm for 20 min at 4 °C. Cell pellets were resuspended in a buffer (50 mM sodium phosphate with pH 8.0, 300 mM NaCl, and 5 mM imidazole supplemented with 0.2 mg/mL lysozyme) and lysed via ultrasonication on ice, followed by centrifugation at 16,000 rpm for 1 h at 4 °C. The resulting supernatant was loaded onto a Ni-affinity chromatography column (Qiagen, Hilden, Germany), and the protein was eluted with a gradient of imidazole (20–300 mM). Protein fractions were collected and concentrated using an Amicon Ultra Centrifugal Filter (Ultracel-3K; Millipore, Darmstadt, Germany), and the hexa-His tag was cleaved with thrombin treatment. The protein was further purified using a Superdex 200 column (GE Healthcare, Piscataway, NJ, USA) pre-equilibrated with a buffer [50 mM Tris-HCl (pH 8.0), and 150 mM NaCl]. Fractions containing the protein were collected and concentrated to 62.9 mg/mL for protein crystallization. Protein purity was assessed by sodium dodecyl sulphate-polyacrylamide gel electrophoresis.

### 2.2. Crystallization and data collection

Protein crystallization conditions were initially explored using Mosquito, a high-throughput crystallization robot (TTP Labtech, UK). Crystallization experiments were conducted on 96-well crystallization plates (Emerald Bio, Bainbridge Island, WA), where each aliquot of crystallization buffers from commercially available kits like MCSG I-IV (Microlytic, Burlington, USA) and PACT (Molecular Dimension, USA) was spread on the plates, using the sitting-drop

vapor-diffusion method. A 300 nL drop of protein solution was mixed with an equal volume of reservoir solution at 20 °C. Crystals were obtained from a crystallization buffer composed of 0.2 M sodium fluoride, 0.1 M Bis-Tris propane (pH 7.5), and 20% PEG 3350 (PACT #G1). Well-shaped crystals were selected and soaked in Perfluoropolyether Cryo Oil (Hampton Research, Aliso Viejo, USA) and flash-frozen in liquid nitrogen. X-ray diffraction data were collected at –178 °C on the BL5C beamline at Pohang Accelerator Laboratory (Pohang, Korea). A total of 100 images were collected with an oscillation range of 1° and exposure time of 1 s per image. Zn atoms in the crystal were identified using Zn anomalous scattering at the K-absorption edge wavelength of Zn. Diffraction data were indexed, processed, and scaled using the HKL2000 program [20]. Detailed information on data collection, including refinement statistics, is presented in [Supplementary Table S1](#).

### 2.3. Structure determination and refinement

The initial phase of PbSI was determined using the MOLREP program [21] embedded in the CCP4i suite [22]. The structure of a sugar isomerase from *Rhizobium meliloti* (PDB code: 3QC0) was used as a template model. A model of PbSI was built manually using Coot [23] and iteratively refined using REFMAC5 [24] and PHENIX [25]. Model refinement was conducted until  $R_{\text{work}}$  and  $R_{\text{free}}$  values reached 21.4% and 27.1%, respectively. The final model was validated using Molprobity [26]. The atomic coordinates and structure factors for the final model have been deposited in the Protein Data Bank under accession code 7VPF.

### 2.4. Size exclusion chromatography-coupled multi-angle light scattering

Size exclusion chromatography-coupled multi-angle light scattering (SEC-MALS) was performed to analyze a multimeric state of PbSI in solution by measuring the absolute molecular weight of PbSI. The purified protein solution was loaded onto a Superdex 200 Increase 10/300 GL 24 mL column, pre-equilibrated with a SEC buffer (20 mM Tris-HCl (pH 8.0), 150 mM NaCl). SEC-MALS was performed at a flow rate of 0.4 mL/min and measurement temperature of 20 °C. A DAWN-TREOS MALS detector for signals was mechanically connected to an ÄKTA Explorer system. The molecular weight of bovine serum albumin in solution was measured as a reference value. Measured data were finally processed using the ASTRA program.

## 3. Results and discussion

### 3.1. Overall structure of PbSI

The crystal structure of PbSI was determined at 2.98 Å resolution. X-ray data collection including Zn anomalous scattering and refinement statistics for PbSI are summarized in [Supplementary Table S1](#). The crystal structure of PbSI revealed that it exists in a dimeric form in the crystallographic environment (Fig. 1A). Each subunit consists of ten α-helices, two  $3_{10}$ -helices, eight β-strands, and several loops (Fig. 1B). Each monomer adopts a TIM barrel fold, in which eight β-strands are surrounded by eight α-helices, forming a barrel shape (Fig. 1B). A Ca ion and a Zn ion were also found in the center of the respective barrels, which are assumed to be the active sites (Fig. 1A and B). We found that several residues in the respective monomers interact with each other (Fig. 1C; gray). Several loops and helices from each monomer are involved in interactions with each other to form the interface (Fig. 1A). Such interactions appear to contribute to structural stability to maintain the dimeric form. Thirty-three residues per monomer, corresponding to 12% of the

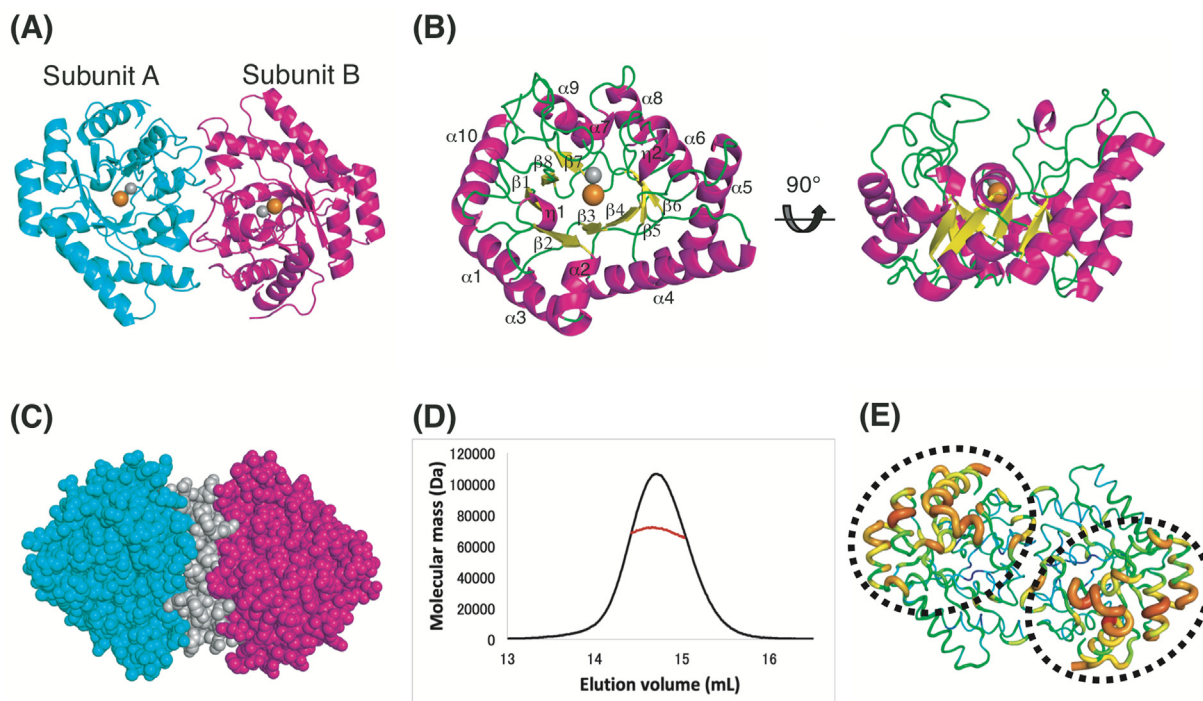


**Fig. 1.** Overall structure of sugar isomerase from *Paenibacillus* sp. R4 (*PbSI*). (A) Dimeric structure of *PbSI*. The structure is represented as a cartoon, and the spheres indicate Ca (yellow) and Zn (gray) ions. (B) Monomeric structure of *PbSI*. The structure in subunit B is represented as a cartoon viewed from two different directions. (C) Interactions between the two subunits of *PbSI*. Interface residues are colored gray. The color code is the same as that of panel (A). (D) Size exclusion chromatography-coupled multi-angle light scattering (SEC-MALS) profile of *PbSI*. SEC-MALS data (red) are plotted as elution volume (x-axis) and molecular mass distributions (y-axis) and are superimposed on the SEC chromatogram (black) at 280 nm. (E) *B*-factor distribution of *PbSI*. The dimeric structure is depicted in putty representation and is rainbow-colored from red to violet in order of *B*-factor value. The dashed ovals indicate regions with high *B*-factor values. (For interpretation of the references to color in this figure legend, the reader is referred to the Web version of this article.)

overall residues, participated in the interface formation.

The multimeric state of SIs in solution is essential for understanding their biological functional units in the cellular environment. A tetramer is a dominant form in most SIs [7–12]. They also exhibit unique structural features to form a tetramer [7–12]. It was found that two molecules in the asymmetric unit form a dimer. The PDBePISA server also suggested a dimeric form as the most probable multimeric state in solution. In addition, we performed SEC-MALS analysis to experimentally verify the dimeric state of *PbSI* in solution. Our SEC-MALS analysis showed that a single peak appeared at the 14.7 mL retention volume, which corresponds to approximately 70 kDa (Fig. 1D). Considering that the theoretical molecular weight of dimeric *PbSI* is approximately 63 kDa, this result indicated that *PbSI* maintains a dimeric form in solution to exert its biological function.

Previous studies have shown that protein mobility may be associated with a determinant of temperature tolerance [27–32]. Hence, the *B*-factor distribution of *PbSI* was analyzed in the dimeric form. The result showed that the dimeric structure of *PbSI* exhibits overall symmetric *B*-factor value distribution (Fig. 1E). Specifically, the outer parts of barrels exhibited relatively high *B*-factor values, corresponding to  $\alpha 1$ ,  $\alpha 3$ ,  $\alpha 9$ , and  $\alpha 10$  helices in the vicinity of the active site (Fig. 1E; dashed ovals). This finding implies that the local mobility of these regions might be associated with the structural plasticity required for catalytic activity at low temperature.

### 3.2. Structure of the active site of *PbSI*

SIs including XIs generally contain two divalent cations such as  $Mg^{2+}$ ,  $Ca^{2+}$ ,  $Mn^{2+}$ ,  $Co^{2+}$ , and  $Zn^{2+}$  in the active site [1,13]. Two

metal ions (M1 and M2) are positioned at their own metal-binding sites [14]. M1 contributes to structural stabilization of the substrate by binding it, and M2 plays a role in facilitating the hydride shift for isomerization of the substrate [14]. However, these metal species are diverse among SIs, and this reflects the chemical specificity for catalysis, depending on the SI type. Therefore, identifying metal species at the active site is necessary for accurately understanding the structure of the active site and the catalytic process.

In the *PbSI* structure, the TIM barrel has a small pocket as the active site, as shown in Fig. 2A. Two metal ions, i.e.,  $Ca^{2+}$  and  $Zn^{2+}$ , are positioned at the bottom of the active site (Fig. 2A). The size of the active site and the metal composition suggest that *PbSI* may bind substrates fitting in the size and that the metal ions play vital roles in catalysis.

Initially, we found that residual electron density maps appeared at the region corresponding to the active site of other homologues (discussed in more detail later). Specifically, this position was assumed to constitute metal sites, such as M1 and M2. Thus, to identify the metal species in the active site, we conducted inductively coupled plasma mass spectrometry (ICP-MS) analysis. Among various elements,  $Mg^{2+}$ ,  $Ca^{2+}$ , and  $Zn^{2+}$  exhibited relatively high concentrations: 352.6 ppb, 475.9 ppb, and 438.5 ppb, respectively (Supplementary Table S2). Thus, these three metal elements were the plausible candidate metal species. Given that two heterogeneous metal ions existed in the same active site, the molar ratio of the two metal ions would be approximately 1:1. Therefore, we provisionally concluded that the two metal ions corresponding to the electron density map are  $Ca^{2+}$  and  $Zn^{2+}$ .

To identify which position in the electron density map corresponds to  $Zn^{2+}$ , we performed X-ray anomalous scattering analysis

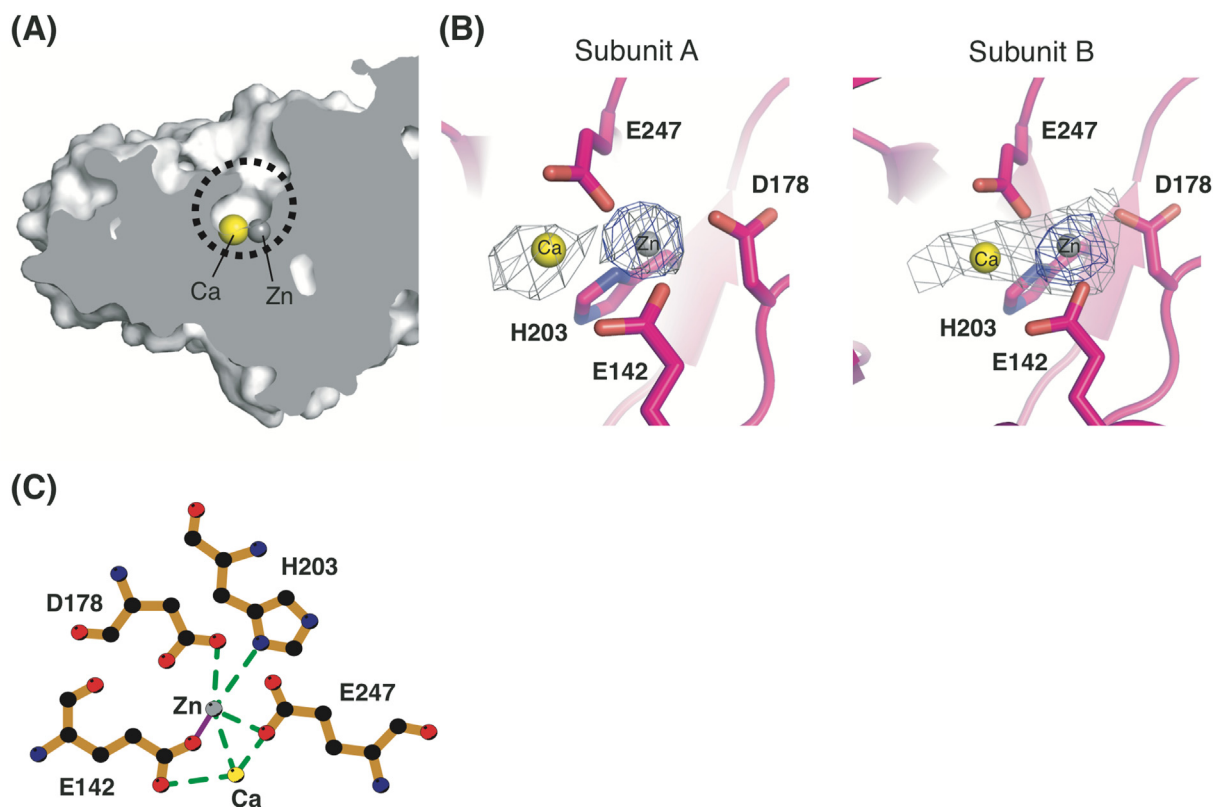


**Fig. 2.** Active site of sugar isomerase from *Paenibacillus* sp. R4 (*PbSI*). (A) A cross-section view representing the active site pocket. Ca (yellow) and Zn (gray) ions are represented as spheres. (B) Omit maps and anomalous difference Fourier maps of the metal ions in subunit A and B. Omit maps ( $m_{F_0-DF_C}$ ) are colored gray and contoured at the  $2.5 \sigma$  (subunit A) and  $2.5 \sigma$  (subunit B) level. The anomalous difference Fourier maps of Zn are colored blue and contoured at the  $10.0 \sigma$  level. (C) Interactions between metal ions and adjacent residues in the active site. Green dashed lines indicate coordinate covalent bonds. (For interpretation of the references to color in this figure legend, the reader is referred to the Web version of this article.)

of Zn, and a wavelength for the K-absorption edge of Zn was investigated and determined to have a value of  $1.2808 \text{ \AA}$ . The  $m_{F_0-DF_C}$  omit maps shown in Fig. 2B (gray) indicate that the residual electron density maps fit the two metal sites. As expected, a Zn ion occupied one of the two positions, and the corresponding map matched approximately half of the omit map (Fig. 2B; blue). Therefore, it is reasonable to assume that the rest of the map indicates the position of a Ca ion. However, the possibility that a Mg ion occupies this position still cannot be excluded.

It was also found that the two metal ions interact with adjacent residues (Fig. 2C). Specifically, the Zn ion electrostatically interacts with the side chains of Glu142, Asp178, His203, and Glu247, including the Ca ion (Fig. 2C). The Ca ion also interacts with Glu142 and Glu247, besides the Zn ion (Fig. 2C). However, it appears that three invisible water molecules are involved in the coordinate covalent bonds to satisfy the coordination number of Ca, which is six. As no substrate or product was clearly observed in our structure, it is difficult to confirm the roles of the two metal ions during the catalytic process. If the Zn ion is involved in the hydride shift, some adjacent residues probably undergo spatial displacements to allow the Zn ion to form an appropriate geometry for catalysis.

### 3.3. Structural comparison with homologues from mesophiles and thermophiles

Considering that *PbSI* is a putative SI from a psychrophile, it may have unique structural features or biophysical properties compared to its homologues, such as SIs from mesophiles and thermophiles. Based on structural similarity and structural information deposited

in the Protein Data Bank, several homologues to *PbSI* were selected as comparison targets: L-xylulose-5-phosphate 3-epimerase UlaE from *E. coli* (PDB ID: 3CQK [33]), xylose isomerase from *Salmonella typhimurium* (PDB ID: 2Q02) as SIs from mesophiles; and xylose isomerase from *Thermoanaerobacterium thermosulfurigenes* (PDB ID: 1AOC), xylose isomerase from *Bacillus stearothermophilus* (PDB ID: 1AOD), xylose isomerase from *Thermus thermophilus* (PDB ID: 1BXB [18]) as SIs from thermophiles. Our structure was compared with these homologues, and structural differences and biophysical properties were analyzed.

We compared the *PbSI* structure with the UlaE structure from *E. coli* (PDB ID: 3CQK), which was well discussed in terms of the key residues for catalysis and its overall structure as a dimer [33]. It was found that the two proteins share the central TIM barrel fold, showing structural variation of several helices and loops adjacent to the active site (Fig. 3A). The root-mean-square deviation value between the two was  $3.21 \text{ \AA}$  over 248 C $\alpha$  atoms. However, the Zn ion and four residues binding it were positioned almost at the same active site (Fig. 3B). In UlaE, the four residues, Glu155, Asp185, His211, and Glu251 coordinate the Zn ion and correspond to Glu142, Asp178, His203, and Glu247 of *PbSI*, respectively (Fig. 3B). Such spatial conservation of the metal and key residues implies that the Zn ion of *PbSI* plays a role similar to that of UlaE in the catalytic process. If our assumption is correct, the Ca ion potentially functions as a substrate stabilizer, and the Zn ion is expected to directly catalyze the hydride shift.

XI from *S. typhimurium* (*StXI*; PDB ID: 2Q02) also has a Zn ion in its active site. As expected, comparison of the structure of *PbSI* with that of *StXI* also revealed that they share the TIM barrel fold in the

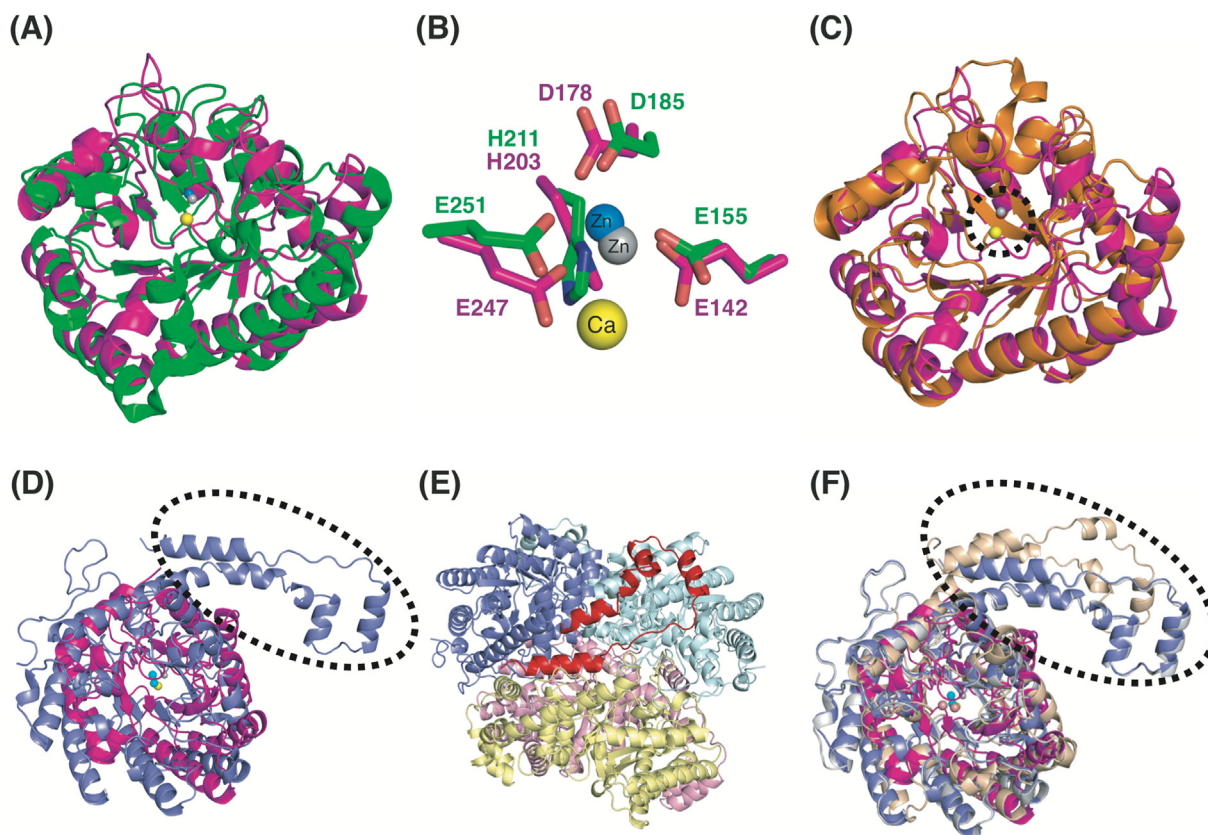


**Fig. 3.** Structural comparison of sugar isomerase from *Paenibacillus* sp. R4 (*PbSI*) with homologues from mesophiles and thermophiles. (A) Overall structural comparison between *PbSI* and *UlaE* from *Escherichia coli*. The structure of *PbSI* (magenta) is superimposed onto that of *UlaE* (green). Ca (yellow) and Zn (gray) ions of *PbSI*, and Zn (blue) ion of *UlaE* are represented as spheres. (B) Comparison of key residues in the active site between *PbSI* and *UlaE*. The color code is the same as that of panel (A). Overall structural comparison between *PbSI* (magenta), *StXI* (C; orange), and *BsXI* (D; slate). The Zn (red) ion of *StXI* and Mn (cyan) ions of *BsXI* are represented as spheres. The black dashed oval in panel (D) indicates the extended C-terminal region of *BsXI*. (E) The tetrameric structure of *BsXI*. The C-terminal region of subunit A (slate) is colored red. (F) Overall structural comparison between *PbSI* (magenta), *BsXI* (slate), *TtsXI* (gray), and *TtXI* (wheat). The Co (pink) ions of *TtsXI* are represented as spheres. The black dashed oval indicates the extended C-terminal regions of *BsXI*, *TtsXI*, and *TtXI*. (For interpretation of the references to color in this figure legend, the reader is referred to the Web version of this article.)

center, and they exhibit spatial differences nearly in the same regions as in *UlaE* (Fig. 3C). Moreover, the position of the Zn ion was almost identical in both (Fig. 3C; dashed circle). This result constituted additional evidence to support our hypothesis concerning the function of the Zn ion of *PbSI*.

Our structure was also compared with the XI from the thermophile *B. stearothersophilus* (*BsXI*; PDB ID: 1A0D). Although the two structures exhibited topological similarity to each other, including the TIM barrel fold, the overall architecture showed substantial spatial deviation (Fig. 3D). Remarkably, it was found that the extended C-terminal region of *BsXI* protrudes out, unlike in the *PbSI* structure (Fig. 3D). Considering that *BsXI* showed a tetrameric form in the crystallographic environment, the C-terminal region of *BsXI* was hook-shaped to connect the subunit to neighboring subunits. Indeed, the C-terminal region was found to interact with two neighboring subunits (Fig. 3E), resulting in the formation of a tight tetramer. This hook-shaped region is commonly observed in other tetrameric SIs, including XI from *T. thermosulfurigenes* (*TtsXI*; PDB ID: 1A0C) and XI from *T. thermophilus* (*TtXI*; PDB ID: 1BXB [18]) (Fig. 3F).

### 3.4. Structural comparison with a homologue from a psychrophile

The crystal structure of an XI from *Paenibacillus* sp. R4 (*PbXI*) has been previously reported. This tetrameric XI has three Ca ions (CaI, CaII, and CaIII) in one subunit, two of which (CaI and CaII) are

positioned in the active site. To investigate structural similarity and differences, *PbSI* and *PbXI* structures were compared. The two proteins showed structural differences like those between *PbSI* and *BsXI* (Fig. 4A). Although they share the TIM barrel fold in the center, *PbXI* has the extended C-terminal region unlike *PbSI* (Fig. 4A).

Moreover, it was found that spatial arrangements of key residues in the active site are different from each other. The four residues (Glu230, Glu266, Asp294, and Asp338) binding the CaI ion in *PbXI* correspond to the four residues (Asp142, Asp178, His203, and Glu247) binding the Zn ion in *PbSI* (Fig. 4B). These residues are well conserved in terms of spatial arrangements. However, residues binding the CaII ion exhibited structural differences from those in *PbSI*. In *PbXI*, the CaII ion is coordinated to Glu266, His269, Asp305, Asp307, and Asp338 (Fig. 4B). Although three residues, Glu266, His269, and Asp338 spatially correspond to Asp178, His181, and Glu247 of *PbSI*, *PbSI* does not have appropriate residues corresponding to Asp305 and Asp307 of *PbXI*. This finding suggests that *PbSI* has its own substrate recognition mode, which is intrinsically different from that of *PbXI*. These structural differences in the spatial arrangements of the metal ions and key residues also imply that *PbSI* may recognize sugar molecules other than xylose.

We also found that the size and shape of the active site are different from each other. The active site of *PbXI* is relatively wide and open, while the active site of *PbSI* is virtually closed (Fig. 4C and D). The active site structure of *PbXI* appeared to be natural as a substrate-free form. However, the active site entrance of *PbSI* was

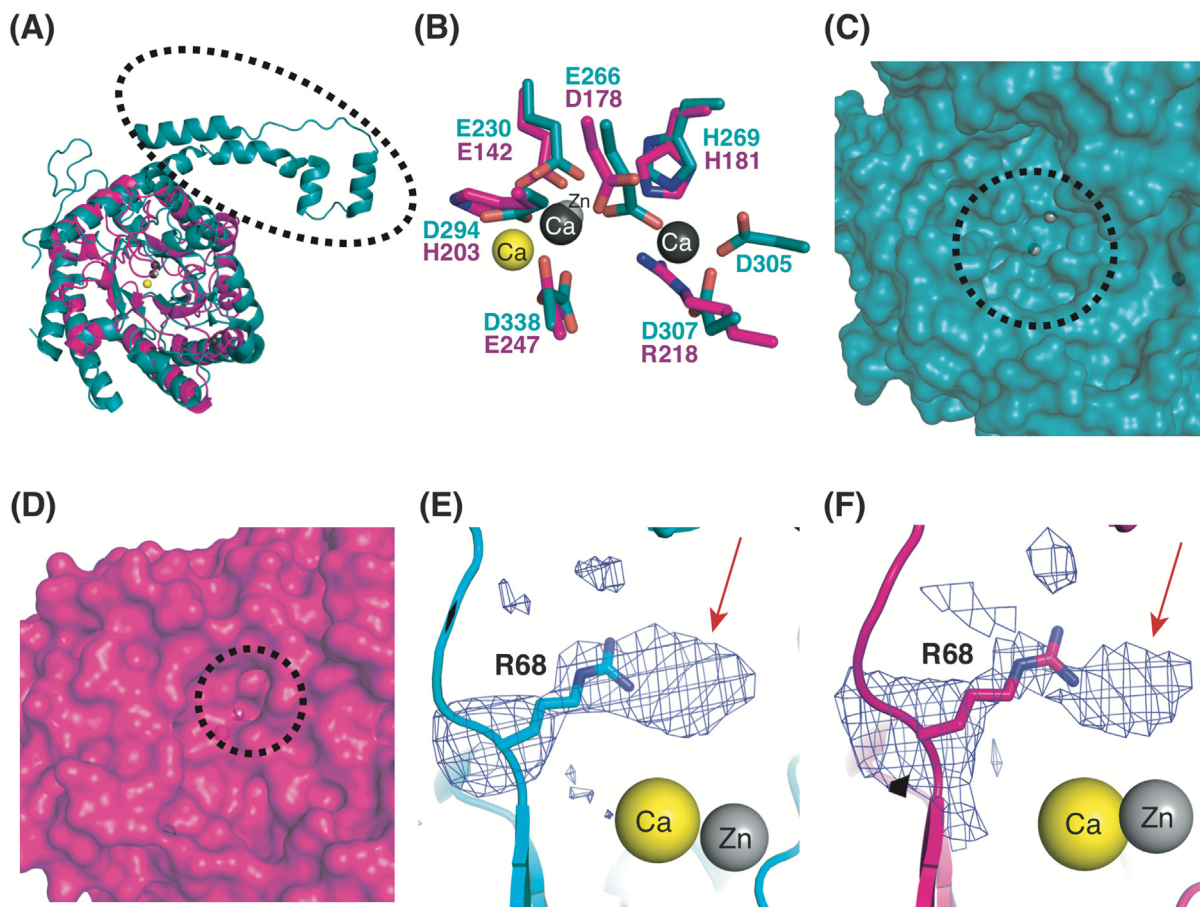


**Fig. 4.** Structural comparison between sugar isomerase from *Paenibacillus* sp. R4 (*PbSI*) and xylose isomerase from *Paenibacillus* sp. R4 (*PbXI*). (A) Overall structural comparison between *PbSI* (magenta) and *PbXI* (teal). Ca (black) ions of *PbXI* are represented as spheres. The black dashed oval indicates extended C-terminal regions of *PbXI*. (B) Comparison of key residues in the active site between *PbSI* and *PbXI*. The color code is the same as that of panel (A). Surface representation of *PbXI* (C) and *PbSI* (D). The dashed circles indicate the respective active site entrances. Omit maps of Arg68 in subunit A (E) and B (F). The respective omit maps ( $mF_o-DF_c$ ) are colored blue and contoured at the  $2.0 \sigma$  level. The red arrows indicate respective residual electron density maps. (For interpretation of the references to color in this figure legend, the reader is referred to the Web version of this article.)

blocked and it appeared to be difficult for external solvent molecules to enter the active site (Supplementary Text S1). Moreover, the  $mF_o-DF_c$  omit map in the proximity of the metal ions in the active site showed that Arg68 potentially bound a molecule, which appears to be the substrate or intermediate of *PbSI* (Fig. 4E and F). Considering that the active site is closed during the catalytic process, our structure may constitute a view showing an intermediate step of the whole catalytic process. Thus, further studies should focus on identifying the substrate of *PbSI* and elucidating its mechanism.

#### Declaration of competing interest

The authors declare that they have no known competing financial interests or personal relationships that could have appeared to influence the work reported in this paper.

#### Acknowledgements

This work was supported by the National Research Foundation of Korea (NRF) grant funded by the Korean government (MSIT) (NRF-2020R1G1A1100765 and NRF-2021M1A5A1075524 (KOPRI-PN21014)). This research was a part of the project titled “Development of potential antibiotic compounds using polar organism resources (15250103, KOPRI Grant PM21030)”, funded by the

Ministry of Oceans and Fisheries, Korea.

#### Appendix A. Supplementary data

Supplementary data to this article can be found online at <https://doi.org/10.1016/j.bbrc.2021.11.026>.

#### References

- [1] S.H. Bhosale, M. B. Rao, V.V. Deshpande, Molecular and industrial aspects of glucose isomerase, *Microbiol. Rev.* 60 (1996) 280–300.
- [2] Z.Q. Liu, W. Zheng, J.F. Huang, L.Q. Jin, D.X. Jia, H.Y. Zhou, J.M. Xu, C.J. Liao, X.P. Cheng, B.X. Mao, Y.G. Zheng, Improvement and characterization of a hyperthermophilic glucose isomerase from *Thermoanaerobacter ethanolicus* and its application in production of high fructose corn syrup, *J. Ind. Microbiol. Biotechnol.* 42 (2015) 1091–1103.
- [3] L.Q. Jin, Q. Xu, Z.Q. Liu, D.X. Jia, C.J. Liao, D.S. Chen, Y.G. Zheng, Immobilization of recombinant glucose isomerase of efficient production of high fructose corn syrup, *Appl. Biochem. Biotechnol.* 183 (2017) 293–306.
- [4] P. Chandrakant, V.S. Bisaria, Application of a compatible xylose isomerase in simultaneous bioconversion of glucose and xylose to ethanol, *Biotechnol. Bioproc. Eng.* 5 (2000) 32.
- [5] P. Chandrakant, V.S. Bisaria, Simultaneous bioconversion of glucose and xylose to ethanol *Saccharomyces cerevisiae* in the presence of xylose isomerase, *Appl. Biochem. Biotechnol.* 53 (2000) 301–309.
- [6] J. Jokela, O. Pastinen, M. Leisola, Isomerization of pentose and hexose sugars by an enzyme reactor packed with cross-linked xylose isomerase crystals, *Enzym. Microb. Technol.* 31 (2002) 67–76.
- [7] M. Whitlow, A.J. Howard, B.C. Finzel, T.L. Poulos, E. Winborne, G.L. Gilliland, A metal-mediated hydride shift mechanism for xylose isomerase based on the

- 1.6 A *Streptomyces rubiginosus* structure with xylitol and D-xylose, *Proteins* 9 (1991) 153–173.
- [8] K.H. Nam, Stable sample delivery in viscous media via a capillary for serial crystallography, *J. Appl. Crystallogr.* 53 (2020) 45–50.
- [9] K.H. Nam, Shortening injection matrix for serial crystallography, *Sci. Rep.* 10 (2020) 107.
- [10] K. Lee, D. Lee, S. Baek, J. Park, S.J. Lee, S. Park, W.K. Chung, J.L. Lee, H.S. Cho, Y. Cho, K.H. Nam, Viscous-medium-based crystal support in a sample holder for fixed-target serial femtosecond crystallography, *J. Appl. Crystallogr.* 53 (2020) 1051–1059.
- [11] K.H. Nam, Polysaccharide-based injection matrix for serial crystallography, *Int. J. Mol. Sci.* 21 (2020) 3332.
- [12] K.H. Nam, Lard injection matrix for serial crystallography, *Int. J. Mol. Sci.* 21 (2020) 5977.
- [13] J.E. Bae, K.Y. Hwang, K.H. Nam, Structural analysis of substrate recognition by glucose isomerase in  $Mn^{2+}$  binding mode at M2 site in *S. rubiginosus*, *Biochem. Biophys. Res. Commun.* 547 (2021) 69–74, 2021.
- [14] T.D. Fenn, D. Ringe, G.A. Petsko, Xylose isomerase in substrate and inhibitor michaelis states: atomic resolution studies of a metal-mediated hydride shift, *Biochemistry* 43 (2004) 6464–6474.
- [15] A.Y. Kovalevsky, L. Hanson, S.Z. Fisher, M. Mustyakimov, S.A. Mason, V.T. Forsyth, M.P. Blakeley, D.A. Keen, T. Wagner, H.L. Carrell, A.K. Katz, J.P. Glusker, P. Langan, Metal ion roles and the movement of hydrogen during reaction catalyzed by D-xylose isomerase: a joint x-ray and neutron diffraction study, *Structure* 18 (2010) 688–699.
- [16] J.E. Bae, I.J. Kim, K.H. Nam, Crystal structure of glucose isomerase in complex with xylitol inhibitor in one metal binding mode, *Biochem. Biophys. Res. Commun.* 493 (2017) 666–670.
- [17] H.L. Carrell, H. Hoier, J.P. Glusker, Modes of binding substrate and their analogues to the enzyme D-xylose isomerase, *Acta Crystallogr. D Biol. Crystallogr.* 50 (1994) 113–123.
- [18] C. Chang, B.C. Park, D.S. Lee, S.W. Suh, Crystal structure of thermostable xylose isomerases from *Thermus caldophilus* and *Thermus thermophilus*: possible structural determinants of thermostability, *J. Mol. Biol.* 288 (1999) 623–634.
- [19] S.H. Park, S. Kwon, C.W. Lee, C.M. Kim, C.S. Jeong, K.J. Kim, J.W. Hong, H.J. Kim, H.H. Park, J.H. Lee, Crystal structure and functional characterization of a xylose isomerases (PbXI) from the psychrophilic soil microorganism, *Paenibacillus* sp, *J. Microbiol. Biotechnol.* 29 (2019) 244–255.
- [20] Z. Otwinowski, W. Minor, Processing of X-ray diffraction data collected in oscillation mode, *Methods Enzymol.* 276 (1997) 307–326.
- [21] A. Vagin, A. Teplyakov, MOLREP: an automated program for molecular replacement, *J. Appl. Crystallogr.* 30 (1997) 1022–1025.
- [22] M.D. Winn, C.C. Ballard, K.D. Cowtan, E.J. Dodson, P. Emsley, P.R. Evans, R.M. Keegan, E.B. Krissinel, A.G. Leslie, A. McCoy, S.J. McNicholas, G.N. Murshudov, N.S. Pannu, E.A. Potterton, H.R. Powell, R.J. Read, A. Vagin, K.S. Wilson, Overview of the CCP4 suite and current developments, *Acta Crystallogr. D Biol. Crystallogr.* 67 (2011) 235–242.
- [23] P. Emsley, K. Cowtan, Coot: model-building tools for molecular graphics, *Acta Crystallogr. D Biol. Crystallogr.* 60 (2004) 2126–2132.
- [24] G.N. Murshudov, P. Skubák, A.A. Lebedev, N.S. Pannu, R.A. Steiner, R.A. Nicholls, M.D. Winn, F. Long, A.A. Vagin, REFMAC5 for the refinement of macromolecular crystal structures, *Acta Crystallogr. D Biol. Crystallogr.* 67 (2011) 355–367.
- [25] P.D. Adams, P.V. Afonine, G. Bunkoczi, V.B. Chen, I.W. Davis, N. Echols, L.W. Headd, L.W. Hung, G.L. Kapral, R.W. Grosse-Kunstleve, A.J. McCoy, N.W. Moriarty, R. Oeffner, R.J. Read, D.C. Richardson, J.S. Richardson, T.C. Terwilliger, P.H. Zwart, PHENIX: a comprehensive Python-based system for macromolecular structure solution, *Acta Crystallogr. D Biol. Crystallogr.* 66 (2010) 213–221.
- [26] V.B. Chen, W.B. Arendall, J.J. Headd, D.A. Keedy, R.M. Immormino, G.J. Kapral, L.W. Murray, J.S. Richardson, D.C. Richardson, MolProbity: all-atom structure validation for macromolecular crystallography, *Acta Crystallogr. D Biol. Crystallogr.* 66 (2010) 12–21.
- [27] S. Kwon, Y. Nishitani, S. Watanabe, Y. Hirao, T. Kanai, H. Atomi, K. Miki, Structure of a [NiFe] hydrogenase maturation protease HylC provides insights into its substrate selectivity, *Biochem. Biophys. Res. Commun.* 498 (2018) 782–788.
- [28] S. Kwon, Y. Nishitani, Y. Hirao, T. Kanai, H. Atomi, K. Miki, Crystal structure of a [NiFe] hydrogenase maturation protease HybD from *Thermococcus kodakarensis* KOD1, *Proteins* 84 (2016) 1321–1327.
- [29] S. Kwon, S. Watanabe, Y. Nishitani, T. Kawashima, T. Kanai, H. Atomi, K. Miki, Crystal structure of a [NiFe] hydrogenase large subunit HyhL in an immature state in complex with a Ni chaperone HypA, *Proc. Natl. Acad. Sci. U.S.A.* 115 (2018) 7045–7050.
- [30] S. Kwon, J.H. Lee, C.M. Kim, H. Jang, H. Yun, J.H. Jeon, I. So, H.H. Park, Structural basis of substrate recognition by a novel thermostable (S)-enantioselective  $\omega$ -transaminase from *Thermomicrobium roseum*, *Sci. Rep.* 9 (2019) 6958.
- [31] S. Kwon, J.H. Lee, C.M. Kim, H.J. Ha, C.S. Lee, J.H. Jeon, I. So, H.H. Park, Structural insights into the substrate specificity of a novel  $\omega$ -transaminase from the thermophilic bacterium *Sphaerobacter thermophilus*, *J. Struct. Biol.* 208 (2019), 107395.
- [32] S. Kwon, C.W. Lee, H.Y. Koh, H. Park, J.H. Lee, H.H. Park, Crystal structure of the reactive intermediate/imine deaminase A homolog from the antarctic bacterium *Psychrobacter* sp. PAMC 21119, *Biochem. Biophys. Res. Commun.* 522 (2020) 585–591.
- [33] R. Shi, M. Pineda, E. Ajamian, Q. Cui, A. Matte, M. Cygler, Structure of L-xylulose-5-phosphate 3-epimerase (UlaE) from the anaerobic L-ascorbate utilization pathway of *Escherichia coli*: identification of a novel phosphate binding motif with a TIM barrel fold, *J. Bacteriol.* 190 (2008) 8137–8144.